



#### **PAPER • OPEN ACCESS**

# Laser-induced organic agglomerates on 2D MoS<sub>2</sub> during thermal treatment

To cite this article: Antun Lovro Brkić et al 2025 Nano Ex. 6 035013

View the article online for updates and enhancements.

# You may also like

- Photonic-digital hybrid artificial intelligence hardware architectures: at the interface of the real and virtual worlds

   When the property of the pro
- Lília M S Dias, Dinis O Abranches, Ana R Bastos et al.
- ICRH modelling of DTT in full power and reduced-field plasma scenarios using full wave codes
- A Cardinali, C Castaldo, F Napoli et al.
- Engineering surface defects on layered PtTe2 and PdTe2 with reacting methanol Jing-Wen Hsueh, Lai-Hsiang Kuo, Wan-Hsin Chen et al.







#### **OPEN ACCESS**

#### RECEIVED

30 December 2024

#### REVISED

18 July 2025

ACCEPTED FOR PUBLICATION 30 July 2025

PUBLISHED

26 August 2025

Original content from this work may be used under the terms of the Creative Commons Attribution 4.0 licence

Any further distribution of this work must maintain attribution to the author(s) and the title of the work, journal citation and DOI.



#### **PAPER**

# Laser-induced organic agglomerates on 2D MoS<sub>2</sub> during thermal treatment

Antun Lovro Brkić<sup>1,2</sup>, Antonio Supina<sup>1</sup>, Davor Čapeta<sup>1</sup>, Lucija Ptiček<sup>3,6</sup>, Livio Racané<sup>3</sup>, Marina Šekutor<sup>4</sup>, Christian Teichert<sup>5</sup>, and Ida Delač<sup>1,\*</sup>

- <sup>1</sup> Centre for Advanced Laser Techniques, Institute of Physics, Bijenička Cesta 46, 10000 Zagreb, Croatia
- Physics Department, Faculty of Mathematics and Physics, University of Ljubljana, Jadranska 19, SI-1000 Ljubljana, Slovenia
- <sup>3</sup> University of Zagreb, Faculty of Textile Technology, Prilaz baruna Filipovića 28a, 10000 Zagreb, Croatia
- Department of Organic Chemistry and Biochemistry, Ruder Bošković Institute, Bijenička 54, 10 000 Zagreb, Croatia
- <sup>5</sup> Chair of Physics, Montanuniversität Leoben, Franz-Josef-Straße 18, 8700 Leoben, Austria
- <sup>6</sup> Current address: Porton PharmaTech, d.o.o., Kolodvorska cesta 27, 1234 Mengeš, Slovenija.
- \* Author to whom any correspondence should be addressed.

E-mail: albrkic@ifs.hr, asupina@ifs.hr, dcapeta@ifs.hr, lucija.pticek@gmail.com, livio.racane@ttf.unizg.hr, msekutor@irb.hr, teichert@unileoben.ac.at and idelac@ifs.hr

**Keywords:** MoS<sub>2</sub> monolayer, chemical vapor deposition (CVD), organic molecules, drop-casting, photoluminescence (PL), Raman spectroscopy, atomic force microscopy (AFM)

#### Abstract

In this study, we investigate the real-time evolution of photoluminescence (PL) in MoS<sub>2</sub> samples modified with L63MS molecules during controlled thermal treatment, unveiling a unique laser-induced molecular agglomeration process. By integrating a heater into our microscopy setup, we monitored *in situ* changes and discovered that between 120 °C and 180 °C, focused laser irradiation induces the formation of molecular agglomerates with heights ranging from 5 to 20 nm (as confirmed by atomic force microscopy (AFM)). Notably, after subsequent heating to 320 °C, while nonagglomerated molecules desorb, these agglomerates remain stable. Raman spectroscopy reveals that the MoS<sub>2</sub> lattice beneath the agglomerates experiences minimal phonon mode shifts—demonstrating a protective effect—and PL measurements show a redshift in the exciton A peak due to localized strain and charge transfer effects. In contrast to previous studies on the real-time PL evolution of MoS<sub>2</sub>, our work uniquely demonstrates that controlled agglomerate formation *via* laser exposure not only modulates optical properties but also provides a pathway for localized functionalization of MoS<sub>2</sub>, opening new avenues for optoelectronic device engineering.

#### 1. Introduction

Two-dimensional (2D) materials, exemplified by graphene and transition metal dichalcogenides (TMDCs) like molybdenum disulfide ( $MoS_2$ ), have gained substantial attention due to their atomic-scale thickness, large surface area, and unique properties [1–4]. These characteristics enable applications in electronics, photonics, catalysis, and energy storage [5–7]. Among these materials, monolayer  $MoS_2$  is particularly notable for its transition to a direct band gap semiconductor, mechanical flexibility, and piezoelectric properties, making it a versatile candidate for optoelectronic and sensing technologies [8–11].

Despite these promising attributes, the practical deployment of MoS<sub>2</sub> and other 2D materials is constrained by their sensitivity to environmental and processing conditions. Their high surface-to-volume ratio and atomic thickness make them prone to defects, degradation, and instability, which can impair device performance [12–14]. To address these challenges, surface modification using organic molecules has emerged as an effective approach to tailor material properties, improve stability, and introduce new functionalities without significantly altering their structural integrity [15–18].

In contrast to previous studies that have focused on the real-time evolution of photoluminescence (PL) spectra in pristine  $MoS_2$  [19, 20], our work presented here uniquely investigates the dynamic behavior of  $MoS_2$ 

modified with organic molecules. By combining controlled thermal treatment with localized laser irradiation, we observe the *in situ* formation of molecular agglomerates that not only modulate the photoluminescence—evidenced by increased PL intensity and a redshift of the exciton A peak—but also serve as protective layers that mitigate thermal strain on the  $MoS_2$  lattice. This dual functionality, involving both tunable optical properties and enhanced structural stability, opens new avenues for locally targeted functionalization and the design of robust optoelectronic devices.

In our previous work, we demonstrated the modification of MoS<sub>2</sub> using the organic molecule 6-(4,5-dihydro-1*H*-imidazol-3-ium-2-yl)-2-(naphthalene-2-yl)benzothiazole methanesulfonate (L63MS) through a simple drop-casting method [21]. This approach allowed property modulation with enhanced stability under ambient conditions. The molecule used is synthesized *via* a green protocol and water-soluble, which simplifies the dispersion and surface interaction processes, thereby providing an efficient, environmentally friendly modification method. The modified MoS<sub>2</sub> samples demonstrated long-term stability, preserving their electronic and optical characteristics under typical environmental exposure. In addition, reversible effects were observed when heating the system above 320 °C, with the desorption of the molecular layer and restoration of the initial optical properties [22]. This thermal reversibility highlights the potential for controlled on-demand tuning of material characteristics.

Although our previous studies have established the behavior of MoS<sub>2</sub> modified with L63MS at room temperature and after thermal treatment above 320 °C, the dynamics of the system during the heating process itself remained unexplored. Key questions include whether the molecules desorb gradually across a range of temperatures or undergo a more abrupt change at specific thresholds, and whether these transitions impact the material's properties. Such *in situ* insights are important for understanding the intermediate states of the system, which could reveal transient molecular rearrangements or interactions that are not apparent in post-heat treatment analyses.

To address this gap, we aimed to monitor the  $L63MS/MoS_2$  system in real time during heating using laser-based techniques such as PL and Raman spectroscopy. Although these methods are nondestructive, they introduce localized heating and laser irradiation, which can influence the material while enabling its characterization. Unexpectedly, we observed the formation of stable molecular agglomerates at the laser focal points during heating, an outcome not anticipated based on prior room-temperature or post-heating studies.

This phenomenon highlights the complex interplay between heating, laser exposure, and molecular modifications on MoS<sub>2</sub>. These findings offer new insights into the thermal and optical responses of the L63MS/MoS<sub>2</sub> system and suggest potential for controlled patterning or functionalization, although through mechanisms that warrant further investigation.

### 2. Materials and methods

To investigate the effects of simultaneous laser irradiation and heating on  $MoS_2$  modified with the organic molecule L63MS, various characterization techniques were employed to analyze morphological and optical changes in the material, including atomic force microscopy (AFM), Raman and PL spectroscopy, and optical microscopy. Below, we detail the synthesis of the materials, sample preparation procedures, and the methods used for characterization and data analysis.

#### 2.1. Synthesis of MoS2 and L63MS

Monolayer  $MoS_2$  was synthesized on a  $SiO_2/Si$  substrate using a chemical vapor deposition (CVD) process, following established protocols described in our previous work [21, 23]. The CVD process resulted in the formation of triangular  $MoS_2$  flakes with sizes ranging from approximately 10  $\mu$ m to 150  $\mu$ m. Detailed characterization in our earlier study [21] confirmed the monolayer nature of these samples, with a typical thickness of  $\approx$ 0.7 nm as measured by AFM and corroborated by the direct bandgap measurements from PL and the characteristic Raman mode separation between  $E_{2g}^1$  and  $A_{1g}$ . The substrate consists of a silicon wafer with a thermally grown  $SiO_2$  layer of about 300 nm thickness.

The organic molecule L63MS was synthesized using a previously reported method involving the Pinner reaction and subsequent condensation with aryl carboxylic acids [24–26]. The molecular structure of L63MS is shown in figure 1. This molecule was chosen due to its water solubility and potential interactions with MoS<sub>2</sub> through non-covalent  $\pi-\pi$  stacking and charge transfer, which may cause structural and electronic changes of MoS<sub>2</sub> layer that will be possibly observed in PL and Raman spectra. Additionally, they could provide a protective layer, improving the material's stability against humidity-induced environmental degradation. Furthermore, this molecular modification may enhance the photostability and charge transport of MoS<sub>2</sub>, which are important for future electronic applications.

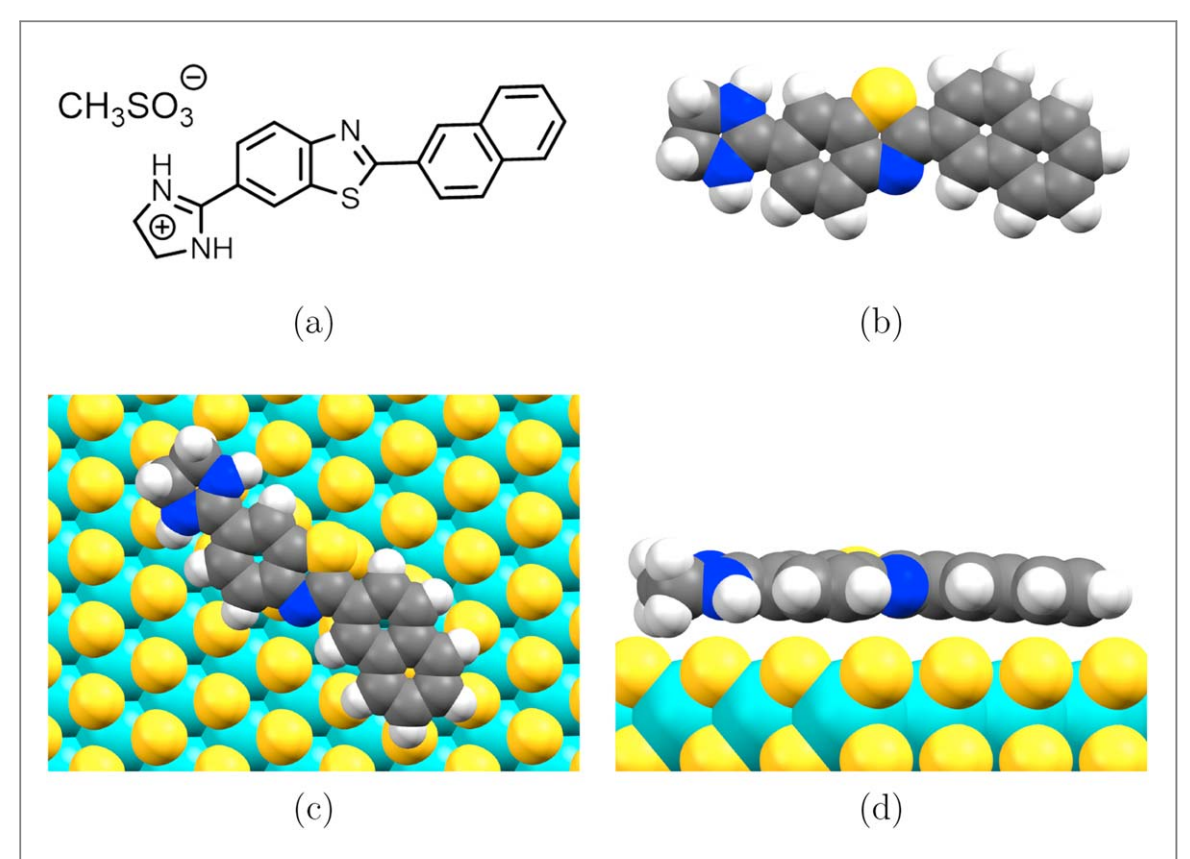


Figure 1. (a) Chemical structure of the L63MS molecule [21]. (b) Optimized geometry of the lone L63MS cation, and optimized geometry of the L63MS cation on  $MoS_2$  post adsorption, top (c) and side view (d).

## 2.2. MoS<sub>2</sub> modification with L63MS

 $MoS_2$  samples were prepared for modification by first cleaning them with isopropanol to remove any surface contaminants. A stock solution of L63MS was prepared by dissolving the molecule in distilled water to a concentration of  $10^{-2}$  M. This stock solution was then diluted with analytical-grade isopropanol to achieve a final concentration of  $10^{-4}$  M.

A volume of 2.5  $\mu L$  of the L63MS solution was drop-cast onto the MoS<sub>2</sub> samples under ambient conditions. The samples were then allowed to dry at room temperature as the solvent evaporated, resulting in the adsorption of L63MS molecules onto the MoS<sub>2</sub> surface.

#### 2.3. Computational analysis

We performed a computational analysis in order to determine how the single L63MS cation adsorbs on the MoS<sub>2</sub> surface (figure 1). Geometry optimization of the lone L63MS cation and the L63MS cation on the MoS<sub>2</sub> surface was done with the semi-empirical quantum mechanical GFN1-xTB method [27, 28] using the xtb version 6.7 implemented in the Orca 6.0 program package [29–31]. The  $10 \times 10$  surface cut-out was constructed from the crystal structure of the 2*H*-MoS<sub>2</sub> phase [32] and the coordinates of the MoS<sub>2</sub> surface were kept frozen during the optimization. For our analysis, we first optimized the lone L63MS cation for comparison purposes using the GFN1-xTB method and the obtained geometry is expectedly planar (figure 1, panel b) due to electron density delocalization along the molecular scaffold. Next we placed one L63MS cation on a pristine surface cutout taken from the 2H-MoS<sub>2</sub> phase crystal structure and optimized its on-surface geometry using the same method. From the resulting adsorbed structure it can be observed that no significant deviation from molecular planarity occurs and the central molecular plane lies practically parallel to the xy plane of the MoS<sub>2</sub> surface (figure 1, panel c and d). The closest points of contact between the surface and the adsorbed molecule are realized through the two C-H moieties on the imidazoline ring. This finding suggests that neither the positively charged imidazoline group nor the sulfur atom contained in the benzothiazole ring have sufficient strength to cause the adsorbed molecule to slant at an angle with respect to the surface. Note, however, that an existence of intrinsic S vacancies and other surface defects of the MoS<sub>2</sub> sample probably leads to additional interactions with the molecule. Additionally, the on-surface presence of the tetrahedral mesylate (CH<sub>3</sub>SO<sub>3</sub>–) counterion during adsorption likely hinders somewhat the ordered stacking of the planar L63MS cation along the z axis.

#### 2.4. Characterization techniques and measurement process

#### 2.4.1. Atomic force microscopy (AFM)

AFM measurements were performed using a commercial AFM system (NanoWizard 4 Ultra Speed, JPK Instruments) operating in tapping mode. Silicon cantilevers with a nominal tip radius of 10 nm (TAP300Al-G, Budget Sensors), a nominal spring constant of 40 N m<sup>-1</sup> and a resonant frequency of 300 kHz were used. The scan rate was set to 1 Hz. AFM was used to obtain high-resolution topographical images of the MoS<sub>2</sub> topography before and after modification. The topography was investigated on both samples before heat treatment and after cooling to room temperature. Surface roughness and agglomerate size were analyzed from the AFM images. AFM characterization was not performed at intermediate temperatures due to the technical limitations of AFM in measuring surfaces undergoing rapid thickness variations caused by temperature oscillations.

#### 2.4.2. Photoluminescence (PL) and Raman spectroscopy

PL and Raman spectra were acquired using a commercial Raman microscope (LabRAM HR Evolution, HORIBA) equipped with a 532 nm excitation laser. The laser was focused using a  $100\times$  objective, yielding a nominal focal spot of approximately  $1.2\mu m$  in diameter—consistent with the lateral dimensions of the laser-induced agglomerates observed in our study. The laser power at the sample was maintained at  $60~\mu W$  throughout the measurements. We performed preliminary power-dependent experiments to verify that this power level is well below the damage threshold for both pristine and L63MS-modified MoS<sub>2</sub> samples; no irreversible damage was observed at or below  $60~\mu W$ , with damage occurring only at substantially higher power levels in accord with [33].

PL spectroscopy was utilized to study the electronic and optical properties of MoS<sub>2</sub>, particularly focusing on excitonic transitions. Due to experimental constraints, we were unable to measure Raman spectra alongside PL at each temperature. Changing the grating to switch from PL to Raman measurements and additional time for the Raman measurement would have required the sample to remain at each temperature for an additional 4–5 min, which could have affected the sample's stability and the accuracy of the temperature-dependent measurements. Due to this restriction, we measured Raman only before and after the heating treatment at room temperature.

#### 2.4.3. Optical microscopy

Optical images of the samples were captured using a metallurgical microscope (DM2700, Leica Microsystems) under white light illumination. Optical microscopy was used to observe the morphology of  $MoS_2$  flakes and to identify regions of interest for further analysis.

#### 2.4.4. Heating setup

A custom heating stage was integrated into the microscope setup to enable simultaneous heating and optical measurements. The stage consisted of a ceramic resistive heater and a thermistor element, both connected to a PID temperature controller and embedded in an aluminum block to maintain uniform temperature. The sample wafer was placed on top of the metallic block, next to an additional thermocouple used to monitor the actual temperature. This temperature control allowed an approximate relative accuracy of 1% at  $300\,^{\circ}$ C. The setup permitted *in situ* measurements of the samples as they were heated. Each temperature change required around  $10\,\mathrm{s}$  of waiting time to allow the heater and sample to reach thermal equilibrium. This waiting period is necessary to compensate for thermal expansion of the heating apparatus and the sample, ensuring that the system remains in focus during measurements.

#### 2.4.5. Experimental procedure

The experimental procedure involved several stages: Baseline Characterization: The as-grown  $MoS_2$  samples were characterized using AFM, Raman spectroscopy, PL spectroscopy, and optical microscopy to establish baseline properties.

Modification with L63MS: The samples were modified by drop-casting the L63MS solution as described above. After drying, the samples were characterized again to assess the effects of the molecular modification. More detailed results can be found in our previous work [21, 22].

Heating and Laser Exposure: The modified samples were placed on the heating stage, and the temperature was increased, starting at 20 °C and ending at 200 °C, with 20 °C increments. PL spectra were recorded in real-time during heating to monitor changes in the optical properties.

Post-Treatment Characterization: After heating and laser exposure, the samples were characterized again using AFM, PL and Raman spectroscopy, and optical microscopy to assess the morphological and optical changes resulting from the treatment.

A L Brkić et al

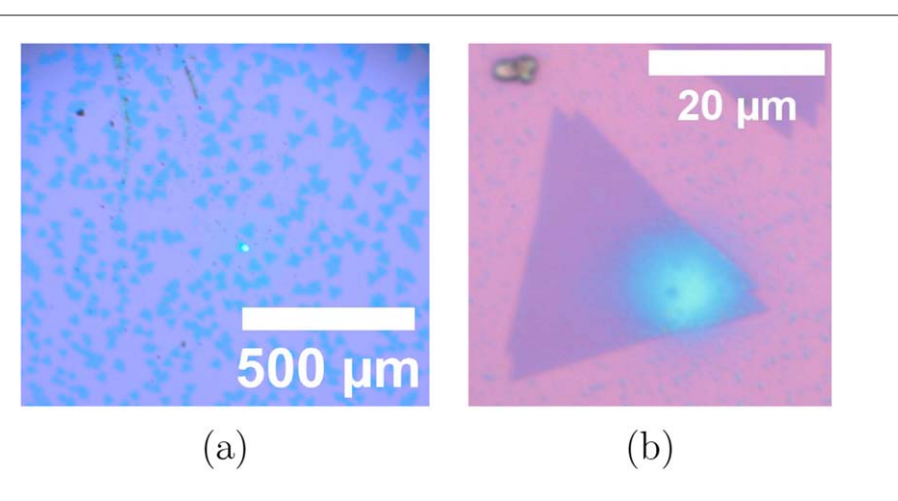


**Figure 2.** Optical microscopy images of the L63MS-modified MoS<sub>2</sub>/SiO<sub>2</sub> surface after completing the array of measurements at different temperatures (20 °C to 200 °C) and subsequent laser exposure. (a) A broader view of the surface showing a newly formed agglomerate as a bright blue spot in the laser-irradiated corner of the MoS<sub>2</sub> triangle. (b) A magnified view of the same region after a total of 60 s of laser exposure at 60  $\mu$ W and 532 nm, illustrating the localized formation of an agglomerate that alters the optical response.

#### 2.5. Data analysis

AFM images were processed and analyzed using Gwyddion software [34]. Surface roughness parameters and agglomerate size were extracted from the images. PL spectra were analyzed using custom Python scripts. Spectra were baseline-corrected, and peaks were fitted using Lorentzian functions to extract peak positions, intensities, and their ratios.

#### 3. Results

#### 3.1. Optical observations of molecular agglomerate formation

Upon heating L63MS-modified MoS $_2$  to elevated temperatures (120 °C–180 °C), we observe distinct optical changes when comparing samples exposed only to heating with those additionally subjected to localized laser irradiation. In regions that experienced both heating and laser exposure, molecular agglomerates form at the laser focal spots. These agglomerates are visible as bright blue-tinted features under an optical microscope, distinguishing them from areas that underwent heating alone. This phenomenon is illustrated in figure 2, where panel (a) highlights a bright blue spot localized on the laser-irradiated corner of the MoS $_2$  triangle, and panel (b) provides a magnified view, revealing the agglomerates formed after 60 s of laser exposure at 60  $\mu$ W and 532 nm.

These observations indicate that, while heating alone does not produce visible surface modifications, the combination of heat and focused laser irradiation appears to induce localized changes on the surface, potentially through molecular clustering. This hypothesis is supported by the pronounced change in optical contrast observed at specific sites. The results suggest that the formation of agglomerates could be spatially and temporally controlled by adjusting the exposure time and laser parameters, although further studies are required to confirm the underlying mechanisms.

### 3.2. AFM characterization of agglomerates and their stability

AFM measurements reveal distinct topographical elevations at the locations of bright optical features, supporting the hypothesis of agglomerate formation. Before laser exposure, the L63MS-modified MoS $_2$  surface exhibits a relatively low roughness of (0.87  $\pm$  0.04) nm. After laser irradiation of 10 s at 120 °C, the surface roughness increases significantly in regions containing agglomerates, reaching (2.75  $\pm$  0.30) nm. Figure 3 illustrates these findings, with panel (a) showing multiple agglomerates protruding from the surface and panel (b) providing cross-sectional profiles that reveal agglomerate heights of approximately 7 nm after 5 s of laser exposure and 17 nm after 10 s. These results demonstrate that the formation and growth of molecular aggregates can be precisely controlled by adjusting laser exposure time.

In addition to controlling the height and growth rate of individual agglomerates through laser exposure parameters, the formation of multiple, spatially separated agglomerates demonstrates the ability to define their placement on the surface. Each newly formed agglomerate appears within the localized region of the laser spot, allowing selective patterning across the  ${\rm MoS_2}$  surface. Moreover, while the heights of the agglomerates vary with exposure time, their lateral dimensions remain relatively stable under these conditions. The agglomerates consistently measure widths around  $(1.2\pm0.2)~\mu{\rm m}$ , which aligns well with the nominal laser spot size of the

A L Brkić et al

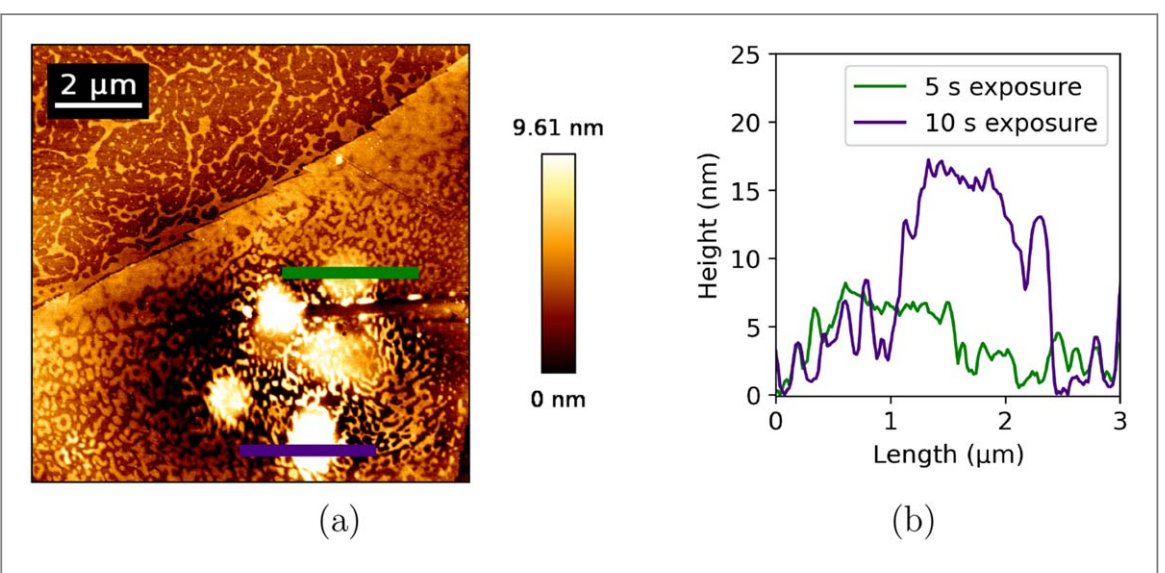


Figure 3. AFM analysis of  $MoS_2/SiO_2$  modified with L63MS molecules after laser exposure at 120 °C. (a) Topography of the surface, showing the presence of molecular agglomerates in the laser-irradiated region. (b) Cross-sectional profiles at exposure times of 5 s (green line) and 10 s (purple line) reveal agglomerate heights of approximately 7 nm and 17 nm, respectively. The surface roughness increases from  $(0.87\pm0.04)$  nm in non-exposed regions to  $(2.75\pm0.30)$  nm in exposed areas, supporting the hypothesis of the direct influence of laser parameters on agglomeration.

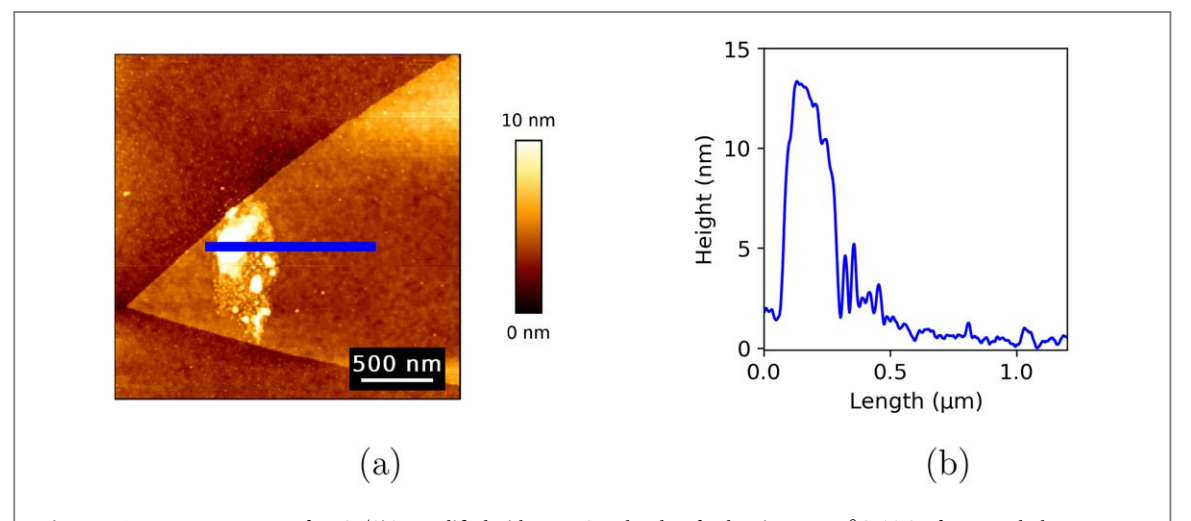


Figure 4. AFM measurements of MoS $_2$ /SiO $_2$  modified with L63MS molecules after heating to 320 °C. (a) Surface morphology highlighting stable agglomerates in laser-exposed regions. (b) Cross-sectional height profile along the indicated line, showing significant roughness in agglomerated areas ((2.76  $\pm$  0.30) nm) compared to non-agglomerated regions ((0.32  $\pm$  0.06) nm). These stable agglomerates remain on the surface despite the high-temperature desorption of non-aggregated molecules.

commercial Raman microscope, equipped with a  $100 \times$  objective. This correspondence supports the interpretation that the lateral extent of the agglomerates is largely determined by the focused laser beam, enabling controlled localized fabrication of stable molecular features on the MoS<sub>2</sub> surface.

Subsequent heating to 320 °C causes non-agglomerated L63MS molecules to desorb from the MoS<sub>2</sub> surface, leaving it nearly pristine [22]. However, agglomerates formed by prior laser exposure remain stable even at these elevated temperatures. AFM measurements after heating to 320 °C (figure 4) show that the agglomerates persist, maintaining elevated roughness values of (2.76  $\pm$  0.30) nm compared to (0.32  $\pm$  0.06) nm in non-agglomerated regions. This stability suggests that aggregated molecular structures act as robust protective layers on the MoS<sub>2</sub> surface.

### 3.3. Temperature-dependent PL and Raman spectroscopy

Having established the morphological changes induced by heating and laser exposure, we now examine their impact on the optoelectronic properties of  $MoS_2$  and their evolution. Figure 5 shows the evolution and the increase of the agglomerates with increased temperatures.

Nano Express **6** (2025) 035013 A L Brkić et al

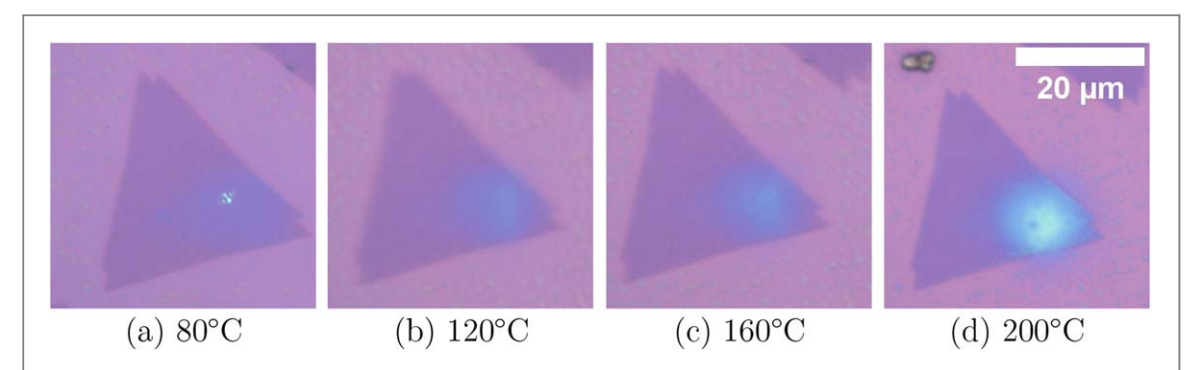
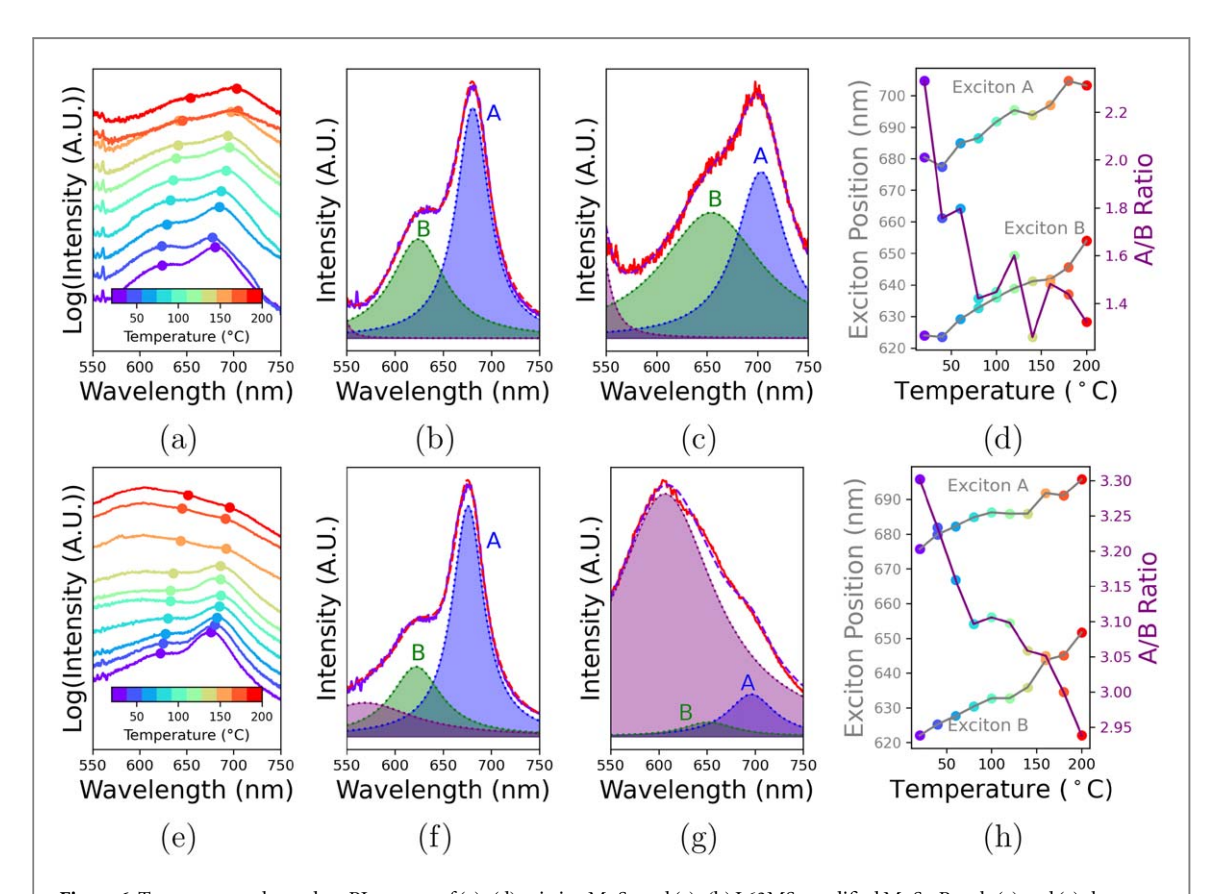


Figure 5. Optical microscopy images showing the temperature-dependent evolution of laser-induced molecular agglomerates on the  $MoS_2/SiO_2$  surface. Images were taken after sequential heating and laser exposure at each temperature. A progressive increase in agglomerate size and optical contrast is observed as the temperature rises from (a) 80 °C to (d) 200 °C, with the agglomerate appearing as an increasingly bright blue region centered on the laser spot.



 $\label{eq:Figure 6.} \begin{tabular}{l} Figure 6. Temperature-dependent PL spectra of (a)-(d) pristine MoS_2 and (e)-(h) L63MS-modified MoS_2. Panels (a) and (e) show log-scale PL spectra from 20 to 200 °C. Panels (b) and (f) show PL at 20 °C with fitted A (in blue) and B (in green) peaks, along with a weak third peak in the modified sample. Panels (c) and (g) show PL at 200 °C, where peaks in pristine MoS_2 broaden and weaken, while the modified sample exhibits a dominant third peak and broad PL features. Panels (d) and (h) summarize exciton A and B positions and A/B intensity ratio, highlighting distinct temperature-dependent behavior caused by molecular modifications, consistent with agglomerate formation.$ 

Figure 6 presents the temperature-dependent PL spectra for pristine MoS<sub>2</sub> (panels a-d) and L63MS-modified MoS<sub>2</sub> (panels e-h). The temperature-dependent behavior of pristine MoS<sub>2</sub>, including the decrease in PL intensity, broadening of excitonic peaks, as well as redshift of the A and B excitonic peaks, is documented in previous studies. These effects have been attributed to enhanced non radiative recombination processes and exciton-phonon interactions at elevated temperatures [19, 35, 36]. As shown in panels (b-d), this characteristic behavior is observed in our measurements as well. The A/B intensity ratio and exciton A and exciton B positions as a function of temperature are summarized in panel (d), further corroborating the temperature-dependent trends reported in earlier research.

The room-temperature total PL intensity of the L63MS-modified MoS<sub>2</sub> is higher than at elevated temperatures (6.f). A broad PL feature emerges at elevated temperatures (120  $^{\circ}$ C–180  $^{\circ}$ C) instead of

A L Brkić et al

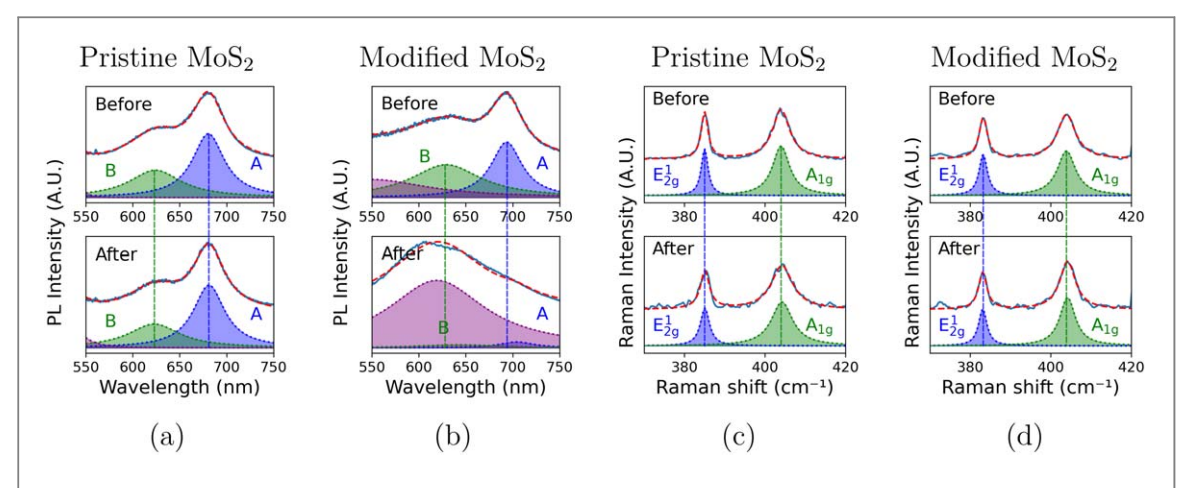


Figure 7. PL and Raman measurements of pristine  $MoS_2(a)$ , (c) and L63MS-modified  $MoS_2(b)$ , (d) before heating and after heating and subsequent cooling. For pristine  $MoS_2(a)$ , (c), both the PL and Raman spectra show minimal changes after the thermal cycle. The  $A_{1g}$  and  $E_{2g}^1$  Raman modes exhibit slight broadening and shifts, consistent with minor lattice distortions and residual strain. In L63MS-modified  $MoS_2(b)$ , (d), the PL signal after cooling (b) is dominated by a broad emission attributed to molecular agglomeration. The Raman spectra (d) show smaller changes in peak positions and widths compared to the pristine sample, indicating that the L63MS molecules mitigate strain and preserve the underlying  $MoS_2$  lattice during the thermal cycle.

diminishing, consistent with the optical and AFM observations of surface agglomerate formation (6.(e,g)). This broad feature is accompanied by the pronounced third peak at 200 °C (6.g), which becomes significantly more intense compared to room temperature.

In addition to *in situ* PL measurement, we measured PL and Raman spectra before and after heating (figure 7) to evaluate the effects of agglomerate formation.

In pristine  $MoS_2$ , the Raman modes (the in-plane  $E_{2g}^1$  and the out-of-plane  $A_{1g}$ ) show slight changes after heating and cooling, indicating subtle effects of thermal treatment on the crystal lattice. The  $A_{1g}$  mode shifts slightly from (385.01  $\pm$  0.02) cm $^{-1}$  to (385.07  $\pm$  0.04) cm $^{-1}$ , while the  $E_{2g}^1$  mode shifts from (403.99  $\pm$  0.03) cm $^{-1}$  to (404.22  $\pm$  0.06) cm $^{-1}$ . Additionally, the widths of both peaks increase, with the  $A_{1g}$  mode broadening from (1.03  $\pm$  0.03) cm $^{-1}$  to (1.38  $\pm$  0.06) cm $^{-1}$ , and the  $E_{2g}^1$  mode broadening from (2.59  $\pm$  0.04) cm $^{-1}$  to (3.22  $\pm$  0.09) cm $^{-1}$ .

The observed broadening of Raman peaks is likely due to residual strain or subtle lattice distortions introduced during the heating and cooling cycle, as well as potential changes in phonon lifetimes. Strain can induce shifts in the frequencies of Raman-active modes, as demonstrated in studies where uniaxial strain applied to monolayer  $MoS_2$  resulted in observable band shifts of the  $E^1_{2g}$  and  $A_{1g}$  modes [37]. Moreover, temperature-dependent studies have shown that anharmonic effects lead to phonon softening and broadening, with phonon-phonon interactions playing a significant role in the temperature dependence of both the frequency and width of Raman modes [38].

For the L63MS-modified sample, the Raman spectra after cooling show smaller changes compared to the pristine sample. The  $A_{1g}$  mode shifts slightly from (383.22  $\pm$  0.03) cm $^{-1}$  to (383.09  $\pm$  0.04) cm $^{-1}$ , while the  $E_{2g}^1$  mode shifts from (403.89  $\pm$  0.04) cm $^{-1}$  to (404.17  $\pm$  0.04) cm $^{-1}$ . Importantly, the peak widths remain unchanged, with the  $A_{1g}$  mode showing no broadening from (1.27  $\pm$  0.04) cm $^{-1}$  to (1.26  $\pm$  0.05) cm $^{-1}$ , and the  $E_{2g}^1$  mode narrowing slightly but insignificantly from (2.75  $\pm$  0.05) cm $^{-1}$  to (2.63  $\pm$  0.06) cm $^{-1}$ . The reduced broadening in the modified sample indicates that the presence of L63MS molecules mitigates strain and protects the underlying MoS $_2$  lattice during the thermal cycle.

The differences in peak broadening between pristine and modified MoS<sub>2</sub> suggest that molecular agglomerates act as protective layers, reducing residual strain and shielding the MoS<sub>2</sub> lattice from thermal stress during heating and cooling.

After thermal treatment and subsequent cooling, PL measurements of the pristine MoS<sub>2</sub> sample shows notable changes in the position and relative intensity of its excitonic peaks. The A exciton peak shifts from (680.45  $\pm$  0.02) nm to (681.16  $\pm$  0.02) nm, while the B exciton shifts slightly from (623.97  $\pm$  0.08) nm to (622.78  $\pm$  0.08) nm. These shifts suggest subtle modifications to the electronic band structure, potentially due to residual strain or defect formation during the thermal cycle. The linewidth of the peaks remain nearly unchanged, with the A exciton narrowing slightly from (20.72  $\pm$  0.04) nm to (20.43  $\pm$  0.04) nm, while the B exciton remains consistent around (33.33  $\pm$  0.19) nm.

The L63MS-modified MoS<sub>2</sub> sample exhibits significant changes in its PL characteristics, dominated by the molecular signatures of agglomerates formed during prolonged exposure. The A exciton peak shifts slightly from (693.38  $\pm$  0.03) nm to (693.74  $\pm$  0.65) nm, and the B exciton shifts from (629.08  $\pm$  0.19) nm to

Nano Express **6** (2025) 035013 A L Brkić et al

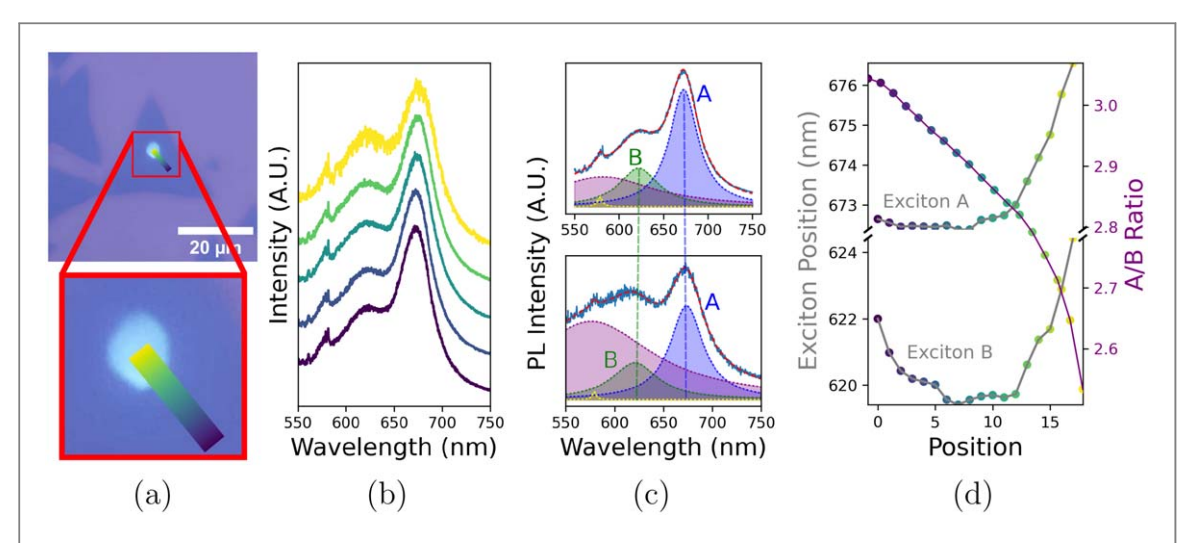


Figure 8. Optical and PL analysis of  $MoS_2/SiO_2$  after thermal treatment at 320 °C. (a) Optical microscopy image showing the laser-irradiated region and the color-coded measurement path across both agglomerated and non-agglomerated areas. (b) PL spectra recorded along the path reveal a gradual redshift of the excitonic peaks and the emergence of molecular emission as the agglomerate center is approached. (c) Fitted PL spectra at two representative positions—far from the agglomerate (top) and at its center (bottom)—demonstrating a clear redshift and enhanced molecular emission at the agglomerate site. (d) Extracted exciton A and B peak positions along the path, along with the corresponding A/B intensity ratio, showing a spatial gradient in optoelectronic properties driven by localized strain and increased molecular density at the agglomerate center.

 $(631.43 \pm 7.51)$  nm. However, these shifts are challenging to assess due to the overwhelming increase in molecular emission, as reflected by the sharp rise in intensity. The molecular signature, represented by the broad agglomerate-associated peak, increases dramatically in intensity from  $(117.61 \pm 1.84)$  to  $(6330.95 \pm 471.14)$ , with a corresponding linewidth broadening from  $(71.22 \pm 2.85)$  nm to  $(56.69 \pm 0.89)$  nm.

This substantial increase in molecular emission dominates the PL spectra, obscuring the relative intensity and precise positions of the  $MoS_2$  excitonic peaks. The A/B intensity ratio becomes difficult to quantify accurately, as the molecular signal overshadows the  $MoS_2$  contributions. These results confirm that prolonged exposure leads to significant molecular agglomeration on the surface, altering the optoelectronic behavior of the modified system and masking the underlying  $MoS_2$  exciton dynamics.

Finally, additional PL measurements taken after heating to 320  $^{\circ}$ C (figure 8) provide insight into the long-term influence of these agglomerates on the MoS<sub>2</sub> optoelectronic properties. This experiment was performed on a different sample, where the surface was exposed to laser irradiation for 30 s at 120  $^{\circ}$ C before being heated to 320  $^{\circ}$ C to remove non-agglomerated molecules. In regions where no agglomerates formed, the desorption of L63MS molecules at high temperature eliminated molecular-induced spectral changes, returning to the values close to those of pristine MoS<sub>2</sub>. This behavior confirms that, without agglomeration, the molecular modifications are neither permanent nor stable under such thermal stress, emphasizing the transient nature of the molecule-substrate interaction in the absence of agglomerate formation. Additional temperature-dependent Raman and PL measurements in our previous work [22] confirm that heating the sample to 320  $^{\circ}$ C effectively desorbs non-agglomerated L63MS molecules. Following the heating process, the characteristic Raman peaks remain unchanged and the exciton A peak shifts from approximately 678 nm to 667 nm, closely matching the emission properties of untreated MoS<sub>2</sub>. Despite some residuals observed by AFM, the optical signatures indicate that the overall MoS<sub>2</sub> lattice returns to an almost pristine state.

The observed redshift of the exciton A peak in the center of the agglomerate, moving from  $(672.65 \pm 0.02)$  nm at the edge to  $(676.56 \pm 0.04)$  nm at the center, can be explained by several factors. One plausible explanation is the presence of strain induced by the molecular agglomeration. Agglomerates can exert localized mechanical strain on the  $MoS_2$  lattice, altering its electronic band structure and leading to the observed redshift of the excitonic features. Strain has been shown to modulate the bandgap of  $MoS_2$ , shifting excitonic peaks depending on the type and magnitude of the strain [39, 40].

The decrease in the A/B intensity ratio, from approximately 3.04 at the edge to 2.53 at the center, suggests a relative reduction in the intensity of the A exciton compared to the B exciton. This could be due to the molecular agglomerates preferentially interacting with the A exciton, causing localized quenching or introducing non-radiative recombination pathways. The A exciton, being closer to the conduction band edge, may be more sensitive to perturbations in the dielectric environment or local energy transfer processes introduced by the molecular agglomerates.

In contrast, the B exciton, originating from transitions involving deeper valence bands, may be less affected by these interactions, thus maintaining a relatively higher intensity at the center. Additionally, energy transfer or

exciton-exciton interactions within the high-density molecular region could preferentially impact the A exciton, further contributing to the decrease in the A/B ratio.

The redshift of the exciton A peak and the decrease in the A/B intensity ratio at the center of the agglomerate likely result from a combination of localized strain effects, enhanced molecular interactions, and differential sensitivity of A and B excitons to their immediate environment.

In figures 6–8, the PL spectra of our samples reveal several key features. The dominant excitonic peaks correspond to the A and B excitons of MoS<sub>2</sub>, which are well-known to arise from direct transitions at the K point, with the B exciton stemming from the spin–orbit splitting of the valence band. In the L63MS-modified samples, we additionally observe a broad emission feature that is absent in pristine MoS<sub>2</sub>. This extra emission can be attributed to the adsorbed molecules and the laser-induced agglomerates, which introduce localized states, modify the dielectric environment, and induce strain. Raman measurements further aid in disentangling these contributions. The characteristic  $E_{2g}^1$  and  $A_{1g}$  phonon modes of MoS<sub>2</sub> remain largely unshifted, indicating that the fundamental lattice structure is maintained. However, subtle differences in the intensity ratios and minor shifts in the excitonic peaks between pristine and modified samples highlight the influence of molecular adsorption. In particular, the localized strain and charge transfer effects induced by the agglomerates are responsible for the observed redshift and variation in the A/B intensity ratio.

In summary, these findings demonstrate that laser-induced molecular agglomerates, formed under moderate heating, are not merely a stable surface feature but also function as controllable modifiers of MoS<sub>2</sub> optical properties. These agglomerates preserve and localize molecule-induced photoluminescence effects, even at elevated temperatures, while simultaneously acting as protective layers for the underlying MoS<sub>2</sub> lattice. Raman measurements confirm that the intrinsic vibrational modes of MoS<sub>2</sub> remain largely unaffected, with minimal peak shifts or broadening, indicating that the agglomerates shield the lattice from strain and environmental perturbations during thermal treatment. Although the agglomerates do not induce significant shifts in intrinsic excitonic transitions, they maintain and spatially localize subtle optical modifications introduced by the molecules. This spatially selective tuning of optoelectronic properties highlights the agglomerates' potential as robust, long-lasting platforms for modifying MoS<sub>2</sub> surfaces. By enabling precise patterning and stability under challenging conditions, this approach opens new avenues for creating tailored molecular architectures that could serve in optical lithography, tunable photonic elements, or targeted functionalization in next-generation 2D device applications.

#### 4. Discussion and conclusion

The findings presented in this work demonstrate how controlled heating combined with localized laser exposure can induce the formation of stable molecular agglomerates on L63MS-modified MoS<sub>2</sub> surfaces. While heating MoS<sub>2</sub> to moderate temperatures (120 °C–180 °C) does not by itself produce optically discernible modifications, the introduction of focused laser irradiation triggers localized transformations in the molecular layer.

The amphiphilic L63MS molecules—with their aromatic naphthalene/benzothiazole cores that readily  $\pi$ – $\pi$  stack—potentially provide the driving force for initial cluster formation [41, 42]. As temperature rises, molecular mobility increases, lowering diffusion barriers and enabling intermolecular attractions, which favor cluster growth [43]. Simultaneously, localized laser heating at the focal spot creates steep temperature gradients that further accelerate surface migration and help overcome molecule—substrate adhesion, yielding stable agglomerates precisely where irradiation occurs [44, 45]. A key observation is that these molecular agglomerates remain stable even after prolonged heating at elevated temperatures (320 °C), outlasting non-agglomerated L63MS molecules that desorb from the MoS<sub>2</sub> surface. The robust nature of these structures suggests that the agglomeration process increases the molecular binding strength and results in structures that are more resistant to high-temperature treatment than individual, non-aggregated molecules. This stability endows the molecular agglomerates with potential as protective layers for MoS<sub>2</sub>, mitigating strain and preserving the underlying lattice structure during thermal cycling.

AFM measurements corroborate the optical data, confirming that the bright optical features arise from elevated topographical structures. The correlation between AFM-derived roughness and optical signatures indicates that these localized molecular assemblies significantly alter the surface properties. Notably, controlling laser parameters (exposure time, intensity) and sample temperature enables the fine-tuning of agglomerate dimensions. The lateral size of the agglomerates remains closely aligned with the laser spot size, underscoring the capacity for direct and spatially selective patterning.

The implications for optoelectronics are equally noteworthy. Unlike pristine  $MoS_2$ , which exhibits characteristic temperature-dependent spectral shifts and a reduction in luminescence intensity at high temperatures, the L63MS-modified samples display distinctive behaviors due to the presence of these molecular clusters. The molecular agglomerates give rise to broad PL features and introduce additional emission peaks that

persist at elevated temperatures. Even after cooling back to room temperature, significant differences remain in the PL and Raman spectra, indicating that the presence of these agglomerates leads to long-lasting alterations in the local photonic environment. The agglomerates influence exciton dynamics by shifting excitonic peak positions and changing exciton intensity ratios—effects that we attribute primarily to localized strain and charge transfer. Furthermore, in line with previous studies, we recognize that PL alterations can also arise from factors such as doping, bandgap modifications, defect healing, impurities, charge traps, and solvent interactions. Therefore, the observed PL changes likely result from a complex interplay between these factors and the laser-induced agglomeration process.

Moreover, these molecular agglomerates appear to function as protective and stabilizing agents during thermal treatment. Raman measurements, which are sensitive to lattice distortions, strain, and curvature-induced effects, reveal that the MoS<sub>2</sub> crystal lattice beneath the agglomerates experiences fewer changes in phonon modes compared to pristine regions. This reduced broadening of Raman peaks and minimal frequency shifts not only point to a protective effect but also suggest that the localized increase in surface roughness and curvature—resulting from molecular adsorption—may subtly influence the phonon behavior. Similar curvature-induced modifications in vibrational properties have been reported in nanostructured materials [46]. Thus, while the aggregated molecules help preserve the intrinsic vibrational characteristics of MoS<sub>2</sub>, they may also contribute to nuanced changes in phonon dispersion through local curvature effects. Further studies are warranted to fully disentangle these contributions.

Another thing to note, our  $MoS_2$  samples were grown by CVD on  $SiO_2/Si$  substrates, which is a system characterized by the close contact between the  $MoS_2$  and  $SiO_2$  that ensures uniform morphology. These relatively uniform interactions, while not directly measured here, are evident from the consistent Raman shifts and the absence of trapped air bubbles, which are often seen in mechanically exfoliated samples. Even though  $SiO_2/Si$  substrates are inherently rough and can induce residual strain, phonon mode distortions, and charge doping effects [47], our AFM and optical data confirm a high-quality, uniform  $MoS_2/Substrate$  interface. However, while it is important to note that the substrate roughness may contribute to the background effects, in our observations laser-induced molecular agglomerates are clearly localized and distinct from these substrate-induced phenomena. Furthermore, we speculate that the effects we observe would be similar for other growth substrates with similar roughness (like SiN or sapphire), but different if 2D  $MoS_2$  would be produced by some other method, for example by exfoliation, but with respect to how the drop-casting would influence the sample, as the interactions between  $MoS_2$  and the substrate would be different, and depositing molecules using the same method could be more challenging. In the future, we plan to expand our research to study both, other growth substrates and also to explore the effects on other 2D materials.

Additionally, the thermal behavior of our  $MoS_2$  samples is also influenced by the substrate and any adsorbed molecules. Although we did not directly measure the thermal expansion coefficients in this study, literature indicates that pristine monolayer  $MoS_2$  typically exhibits a thermal expansion coefficient of approximately  $7 \times 10^{-6} \, K^{-1}$ . The presence of adsorbed molecules can further modify the local thermal expansion and induce additional strain. These substrate-induced effects, combined with the intrinsic properties of  $MoS_2$ , contribute to the overall optoelectronic response and must be considered when interpreting the results. The 10 s waiting period employed in our setup ensures that the system reaches a steady thermal state, thereby minimizing transient thermal effects during optical measurements.

From a technological perspective, the capacity to controllably form and pattern stable molecular agglomerates on MoS<sub>2</sub> suggests new avenues for nanoscale lithography, localized modification, and tunable optoelectronic device engineering. The ability to create spatially localized modifications that remain stable under challenging conditions provides a powerful tool for tailoring the properties of 2D materials without degrading their intrinsic qualities. Such stable, patterned molecular architectures could be leveraged to design optical elements with controlled emission, serve as protective coatings for electronic or photonic components, or act as localized chemical modification sites for sensors, catalysis, or other device applications.

In conclusion, this study establishes that molecular agglomerates formed under combined heating and laser irradiation on  $MoS_2$  surfaces are not only optically and topographically distinct but also structurally robust and optoelectronically active. These agglomerates protect the underlying lattice, preserve molecule-induced optical signatures, and impart long-lasting modifications to  $MoS_2$ . By enabling precise, localized control over molecular clustering, this approach paves the way for patterned, stable, and tunable functionalization of 2D materials. Moreover, while this study focused on only one molecular species, similar organic molecules with comparable binding properties might exhibit analogous behavior, for which further experiments are required to generalize the phenomenon. While laser-induced molecular agglomeration on  $MoS_2$  remains an emerging area with limited direct comparisons, our findings align with prior studies on  $MoS_2$  modifications. The ability to achieve controlled, stable molecular agglomeration opens up exciting possibilities for nanoscale patterning and lithographic applications on  $MoS_2$ . Future research will aim to elucidate the precise molecular mechanisms

underlying agglomeration, explore the influence of different molecular species, and leverage these findings for the targeted design of advanced 2D devices.

# Acknowledgments

This work was supported by the Croatian Science Foundation under the project number HRZZ-UIP-2020-02-8891; Center of Excellence for Advanced Materials and Sensing Devices, ERDF Grant No. KK.01.1.1.01.0001. and Centre for Advanced Laser Techniques, ERDF Grant KK.01.1.1.05.0001. co-financed by the European Union through the European Regional Development Fund—Competitiveness and Cohesion Operational Program and the Croatian Government. Also, the bilateral Croatian-Austrian project funded by Croatian Ministry of Science and Education and the Centre for International Cooperation and Mobility (ICM) of the Austrian Agency for International Cooperation in Education and Research (OeAD-GmbH) under project HR 02/2020 is acknowledged. The computations were performed on the HPC Supek based in SRCE—University of Zagreb, University Computing Centre for computational resources.

#### Conflict of interest

The authors declare no conflict of interest.

# Data availability statement

All the relevant data is already contained within the paper. Also, presented research is part of yet undefended PhD thesis, so the raw data that support the findings of this study are available upon reasonable request from the authors.

#### **Author contributions**

Antun Lovro Brkić 0 0000-0002-0891-6246

Conceptualization (equal), Data curation (lead), Formal analysis (lead), Investigation (equal), Software (equal), Validation (equal), Visualization (lead), Writing – original draft (lead), Writing – review & editing (equal)

Antonio Supina

Conceptualization (equal), Investigation (equal), Software (equal), Validation (equal), Writing – original draft (supporting), Writing – review & editing (supporting)

Davor Čapeta

Methodology (equal), Resources (equal)

Lucija Ptiček

Methodology (equal), Resources (equal)

Livio Racané

Resources (equal), Supervision (equal)

Marina Šekutor © 0000-0003-1629-3672

Formal analysis (supporting), Investigation (supporting), Methodology (equal), Software (equal), Visualization (supporting), Writing – review & editing (supporting)

Christian Teichert 00000-0002-0796-2355

Funding acquisition (equal), Project administration (supporting), Supervision (equal), Writing – review & editing (supporting)

Ida Delač 10 0000-0002-7481-6542

Conceptualization (supporting), Funding acquisition (equal), Project administration (lead), Resources (equal), Supervision (lead), Writing – review & editing (equal)

#### References

- [1] Novoselov K S, Geim A K, Morozov S V, Jiang D, Zhang Y, Dubonos S V, Grigorieva I V and Firsov A A 2004 Electric field effect in atomically thin carbon films *Science* 306 666–9
- [2] Splendiani A, Sun L, Zhang Y, Li T, Kim J, Chim C-Y, Galli G and Wang F 2010 Emerging photoluminescence in monolayer MoS<sub>2</sub> Nano Lett. 10 1271–5
- [3] Liu X, Balla I, Bergeron H and Hersam M C 2016 Point defects and grain boundaries in rotationally commensurate MoS<sub>2</sub> on epitaxial graphene J. Phys. Chem. C 120 20798–805
- [4] Liu Y, Huang Y and Duan X 2019 Van der Waals integration before and beyond two-dimensional materials Nature 567 323–33
- [5] Akinwande D et al 2017 A review on mechanics and mechanical properties of 2D materials—graphene and beyond Extreme Mechanics Letters 13 42–77
- [6] Wang Q H, Kalantar-Zadeh K, Kis A, Coleman J N and Strano M S 2012 Electronics and optoelectronics of two-dimensional transition metal dichalcogenides Nat. Nanotechnol. 7 699–712
- [7] Kim J H, Jeong J H, Kim N, Joshi R and Lee G-H 2018 Mechanical properties of two-dimensional materials and their applications J. Phys. D: Appl. Phys. 52 083001
- [8] Mak K F, Lee C, Hone J, Shan J and Heinz T F 2010 Atomically thin  $MoS_2$ : a new direct-gap semiconductor *Phys. Rev. Lett.* 105 2–5
- [9] Kuc A, Zibouche N and Heine T 2011 Influence of quantum confinement on the electronic structure of the transition metal sulfide TS<sub>2</sub> Phys. Rev. B 83 245213
- $[10]\ Bertolazzi\,S, Brivio\,J\, and\, Kis\,A\,2011\, Stretching\, and\, breaking\, of\, ultrathin\, MoS_2\, ACS\, Nano\, {\color{red}5}\,9703-9\, {\color{gray}0}\, {\color{gray}0}\,$
- [11] Wu W et al 2014 Piezoelectricity of single-atomic-layer MoS<sub>2</sub> for energy conversion and piezotronics Nature 514 470-4
- [12] Tao H, Zhang Y, Gao Y, Sun Z, Yan C and Texter J 2017 Scalable exfoliation and dispersion of two-dimensional materials—an update Phys. Chem. Chem. Phys. 19921–60
- [13] Cai X, Luo Y, Liu B and Cheng H-M 2018 Preparation of 2D material dispersions and their applications Chem. Soc. Rev. 47 6224-66
- [14] Huo C, Yan Z, Song X and Zeng H 2015 2D materials via liquid exfoliation: a review on fabrication and applications Sci. Bull. 60 1994–2008
- [15] Kuila T, Bose S, Mishra A K, Khanra P, Kim N H and Lee J H 2012 Chemical functionalization of graphene and its applications Prog. Mater. Sci. 57 1061–105
- [16] Bottari G, Herranz M, Wibmer L, Volland M, Rodrìguez-Pérez L, Guldi D M, Hirsch A, Martin N, D'Souza F and Torres T 2017 Chemical functionalization and characterization of graphene-based materials Chem. Soc. Rev. 46 4464–500
- [17] Yu W, Sisi L, Haiyan Y and Jie L 2020 Progress in the functional modification of graphene/graphene oxide: a review RSC Adv. 10 15328–45
- [18] Li H, Pam M E, Shi Y and Yang H Y 2017 A review on the research progress of tailoring photoluminescence of monolayer transition metal dichalcogenides FlatChem 4 48–53
- [19] Ibrahim W L, Öper M, Şar H, Ay F and Perkgöz N K 2022 Evolution of Raman and photoluminescence spectral characteristics of monolayer CVD-MoS<sub>2</sub> over a wide temperature range Vib. Spectrosc. 123 103443
- [20] Dong M, Young R J, Dunstan D J and Papageorgiou D G 2023 Interfacial stress transfer in monolayer and few-layer MoS<sub>2</sub> nanosheets in model nanocomposites Compos. Sci. Technol. 233 109892
- [21] Brkić A L, Supina A, Čapeta D, Dončević L, Ptiček L, Mandić, Racané L and Delač I 2023 Influence of solvents and adsorption of organic molecules on the properties of CVD synthesized 2D MoS<sub>2</sub> Nanomaterials 13 2115
- [22] Brkić A L, Supina A, Čapeta D, Dončević L, Ptiček L, Mandić Š., L. Racané L and I. Delač I 2024 Stability and reversibility of organic molecule modifications of CVD-synthesized monolayer MoS2 Nanotechnology 36 065702
- [23] Delač Marion I, Čapeta D, Pielić B, Faraguna F, Gallardo A, Pou P, Biel B, Vujičić N and Kralj M 2018 Atomic-scale defects and electronic properties of a transferred synthesized MoS<sub>2</sub> monolayer Nanotechnology 29 305703
- [24] Racané L, Ptiček L, Sedić M, Grbčić P, Kraljević Pavelić S, Bertoša B, Sović I and Karminski-Zamola G 2018 Eco-friendly synthesis, in vitro anti-proliferative evaluation, and 3D-QSAR analysis of a novel series of monocationic 2-aryl/heteroaryl-substituted 6-(2-imidazolinyl)benzothiazole mesylates Mol. Diversity 22 723–41
- [25] Racané L, Ptiček L, Fajdetić G, Tralić-Kulenović V, Klobučar M, Kraljević Pavelić S, Perić M, Čipčić Paljetak H, Verbanac D and Starčević K 2020 Green synthesis and biological evaluation of 6-substituted-2-(2-hydroxy/methoxy phenyl)benzothiazole derivatives as potential antioxidant, antibacterial and antitumor agents Bioorg. Chem. 95 103537
- [26] Ptiček L, Hok L, Grbčić P, Topić F, Cetina M, Rissanen K, Kraljević Pavelić S, Vianello R and Racané L 2021 Amidino substituted 2-aminophenols: biologically important building blocks for the amidino-functionalization of 2-substituted benzoxazoles Org. Biomol. Chem. 19 2784–93
- [27] Grimme S, Bannwarth C and Shushkov P 2017 A robust and accurate tight-binding quantum chemical method for structures, vibrational frequencies, and noncovalent interactions of large molecular systems parametrized for all spd-block elements (Z = 1-86)

  J. Chem. Theory Comput. 13 1989–2009
- [28] Bannwarth C, Caldeweyher E, Ehlert S, Hansen A, Pracht P, Seibert J, Spicher S and Grimme S 2020 Extended tight-binding quantum chemistry methods WIREs Comput. Mol. Sci. 11 e1493
- [29] Neese F 2012 The ORCA program system WIREs Comput. Mol. Sci. 273–8
- [30] Neese F, Wennmohs F, Becker U and Riplinger C 2020 The ORCA quantum chemistry program package J. Chem. Phys. 152 L224108
- [31] Neese F 2022 Software update: the ORCA program system, version 5.0 WIREs Comput. Mol. Sci. 12 e1606
- [32] Schönfeld B, Huang J J and Moss S C 1983 Anisotropic mean-square displacements (MSD) in single-crystals of 2H- and 3R-MoS<sub>2</sub> Acta Crystallogr., Sect. B 39 404–7
- [33] Solomon J M, Ahmad S I, Dave A, Lu L-S, HadavandMirzaee F, Lin S-C, Chen S-H, Luo C-W, Chang W-H and Her T-H 2022 Ultrafast laser ablation, intrinsic threshold, and nanopatterning of monolayer molybdenum disulfide *Sci. Rep.* 12 6910
- [34] Nečas D and Klapetek P 2012 Gwyddion: An open-source software for SPM data analysis *Open Phys.* 10 181–188
- [35] Tan L, Yang M-M, Hu X-W, Yan Q-G, Wu C-L, Liang B-L, Zhang Y and Li X-L 2023 Temperature-dependent photoluminescence characteristics of 2D vertically oriented MoS<sub>2</sub> microsheets grown by magnetron sputtering Optik 288 171188
- [36] Molina-Sánchez A, Palummo M, Marini A and Wirtz L 2016 Temperature-dependent excitonic effects in the optical properties of single-layer MoS<sub>2</sub> Phys. Rev. B 93 155435
- [37] Rice C, Young R J, Zan R, Bangert U, Wolverson D, Georgiou T, Jalil R and Novoselov K S 2013 Raman-scattering measurements and first-principles calculations of strain-induced phonon shifts in monolayer MoS<sub>2</sub> Phys. Rev. B. Condens. Matter Mater. Phys. 87 1–5 081307(R)
- [38] Sarkar S et al 2020 Anharmonicity in Raman-active phonon modes in atomically thin MoS<sub>2</sub> Phys. Rev. B 101 205302

Nano Express **6** (2025) 035013 A L Brkić et al

[39] Peng Z, Chen X, Fan Y, Srolovitz DJ and Lei D 2020 Strain engineering of 2D semiconductors and graphene: from strain fields to band-structure tuning and photonic applications *Light: Science & Applications* 9 190

- [40] Wang C, Li S, Wang S, Zhao P and Zhuo R 2022 First principles study of the effect of uniaxial strain on monolayer MoS<sub>2</sub> *Physica E* 144 115401
- [41] Carter-Fenk K and Herbert J M 2020 Reinterpreting π-stacking Phys. Chem. Chem. Phys. 22 24870–86
- [42] Cho H J, Kim S W, Kim S, Lee S, Lee J, Cho Y, Lee Y, Lee T-W, Shin H-J and Song C 2020 Suppressing  $\pi-\pi$  stacking interactions for enhanced solid-state emission of flat aromatic molecules via edge functionalization with picket-fence-type groups *J. Mater. Chem. C* 8 17289–96
- [43] Wang J, Li Z, Jia Y, Wang B and Xu Z 2021 Molecular dynamics simulation of effect of temperature on Cu nanoparticles agglomeration of nanofluids *J. Nanopart. Res.* 23 28
- [44] Sekkat Z 2022 Enhancement of molecular mobility in solid polymers by light: fundamentals and applications Appl. Phys. B 128 19
- [45] Wetzel F, Rönicke S, Müller K, Gyger M, Zink M and Käs J 2011 Single cell viability and impact of heating by laser absorption Eur. Biophys. J. 40 1109–14
- [46] Kahaly M U and Waghmare U V 2008 Effect of curvature on structures and vibrations of zigzag carbon nanotubes: a first-principles study Bull. Mater. Sci. 31 335–41
- [47] Chae W H, Cain J D, Hanson E D, Murthy A A and Dravid V P 2017 Substrate-induced strain and charge doping in CVD-grown monolayer MoS<sub>2</sub> Appl. Phys. Lett. 111 143106